J. Non-Newtonian Fluid Mech. 165 (2010) 1–13

Contents lists available at ScienceDirect

Journal of Non-Newtonian Fluid Mechanics

journal homepage: www.elsevier.com/locate/jnnfm

Flow of wormlike micelle solutions through a periodic array of cylinders

Geoffrey R. Moss, Jonathan P. Rothstein*

Department of Mechanical and Industrial Engineering, University of Massachusetts, Amherst, MA 01003, USA

ARTICLE INFO

Article history:
Received 10 November 2008
Received in revised form 15 May 2009
Accepted 10 August 2009

Keywords:
Periodic array of cylinders
Wormlike micelle solution
Viscoelastic
PIV
FIB

ABSTRACT

Solutions of self-assembled wormlike micelles are used with ever increasing frequency in a multitude of consumer products ranging from cosmetic to industrial applications. Owing to the wide range of applications, flows of interest are often complex in nature; exhibiting both extensional and shear regions that can make modeling and prediction both challenging and valuable. Adding to the complexity, the micellar dynamics are continually changing, resulting in a number of interesting phenomena, such as shear banding and extensional flow instabilities. In this paper, we present the results of our investigation into the flow fields generated by a controllable and idealized porous media: a periodic array of cylinders. Our test channel geometry consists of six equally spaced cylinders, arranged perpendicular to the flow. By systematically varying the Deborah number, the flow kinematics, stability and pressure drop were measured. A combination of particle image velocimetry in conjunction with flush mount pressure transducers were used to characterize the flow, while flow induced birefringence measurements were used to determine micelle deformation and alignment. The pressure drop was found to decrease initially due to the shear thinning of the test fluid, and then exhibit a dramatic upturn as other elastic effects begin to dominate. We present evidence of the onset of an elastic instability in one of the test fluids above a critical Deborah number manifest in fluctuating transient pressure drop measurements and asymmetric streamlines. We argue that this disparity in the two test fluids can be attributed to the measurable differences in their extensional rheology.

1. Introduction

Viscoelastic wormlike micelle solutions are currently being used extensively as rheological modifiers in consumer products such as paints, detergents, pharmaceuticals, lubricants and emulsifiers where careful control of the fluid properties are required. In addition, micelle solutions have also become important in a wide range of applications including agrochemical spraying, inkjet printing, turbulent drag reduction and enhanced oil recovery where they are often used as a polymer-free fracture fluid for stimulating oil production [1–3]. A fundamental understanding of the behavior of these complex fluids in different flow regimes is therefore extremely important to a host of industries. Techniques for the analysis and control of the flow of complex fluids require accurate determination of material properties as well as the ability to understand and predict changes that occur within the materials as they are subjected to the flow conditions encountered in industrial and commercial applications. Shear and extensional rheometers provide an excellent framework for investigating the behavior of these complex fluids because the flow kinematics tends to be simple. Additionally, these rheological measurements can shed light on the dynamics of wormlike micelle solutions in complex flows and phenomena such as elastic flow instabilities, which commonly occur in many of the industrial and commercial applications mentioned above. A number of studies of the nonlinear rheology and the behavior of these complex fluids in strong flows have recently been published. To date, no study has been performed on the response of solutions of wormlike micelles through a periodic array of cylinders.

Surfactants are amphiphilic molecules which have both a bulky hydrophilic head, which is often charged, and a relatively short and slender hydrophobic tail typically consisting of an 8-20 carbon atom chain. Above their critical micelle concentration (CMC), surfactant molecules in water will spontaneously self-assemble into large aggregates known as micelles to minimize the exposure of their tails to water [4–6]. In oil, reverse micelles are formed where instead the head-groups are shielded from the oil [7,8]. As seen in Fig. 1, these large aggregates can form into a number of different complex shapes including spherical and wormlike micelles, vesicles and lipid bilayers [9]. The morphology of the aggregates depends on the size of the surfactant head group, the length and number of tails, the charge on the surfactant, the salinity of the solution, temperature, and the flow conditions [4,9]. We are most interested in wormlike micelle because as suggested by their pseudonym 'living polymers,' wormlike micelles display many of the same viscoelastic properties of polymers. However,

* Corresponding author.
E-mail address: rothstein@ecs.umass.edu (J.P. Rothstein).

0377-0257/$ – see front matter © 2009 Elsevier B.V. All rights reserved.
doi:10.1016/j.jnnfm.2009.08.007

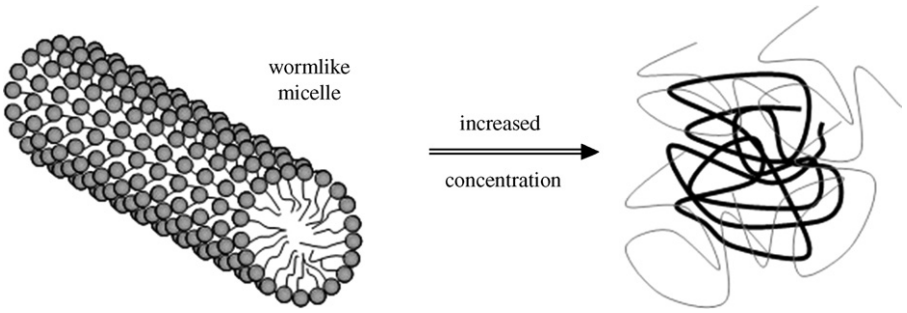

Fig. 1. Schematic diagram of a wormlike micelle.

although both wormlike micelle solutions and polymer solutions can be viscoelastic, wormlike micelles are physically quite different from polymers. Whereas the backbone of a polymer is covalently bonded and rigid, wormlike micelles are held together by relatively weak physical attractions and as a result are continuously breaking and reforming with time. In an entangled network, both individual polymer chains and wormlike micelles can relieve stress through reptation driven by Brownian motion [5]. However, unlike polymeric fluids, wormlike micelle solutions have access to a number of stress relief mechanisms in addition to reptation. Wormlike micelles can relieve stress and eliminate entanglement points by either breaking and reforming in a lower stress state [6] or alternatively by creating a temporary branch point which allows two entangled micelles to pull right through each other thereby eliminating the entanglement point and relieving stress in what has become known as a 'ghost-like' crossing [10]. Additionally, the constant re-organization of the network structure results in several interesting phenomenon when subjected to strong flows. Under all but the most extreme conditions, the large viscosities of these solutions lead to vanishingly small Reynolds number, $Re = UL/\nu$ where U is the mass averaged velocity, L is a characteristic length scale, and ν is the fluid's viscosity. In all of the experiments presented herein, the Reynolds number was of order $Re \leq 10^{-3}$ or smaller.

One such phenomenon subject to much interest and research in recent years is that of shear banding. This flow induced structural change is the result of the micellar network coexisting at two distinct shear rates under an applied stress. When subjected to a shear flow above a critical stress, such as those generated by a cylindrical Couette geometry, the micellar solution responds by forming two or more bands, each flowing at a distinct shear rate such that the fluid experiences a constant average rate of strain across the geometric gap it fills. There have been several elucidatory investigations into this behavior, making use of mechanical and optical measurement techniques [11,12]. Another interesting feature of wormlike micelles is their mechanism of mechanical failure under an applied stress. Flow curves have shown these solutions to be both shear thinning [6], and strain hardening in extensional flows [13]. However, measurements of these non-Newtonian behaviors are not predictive of their method of failure in extensional flows. In extensional flow, fluid filaments of wormlike micelle solutions were observed to fail dramatically at mid plane after accumulating a significant amount of extensional stress. This behavior has been observed most recently by Bhardwaj et al. [14], and is believed to be caused by a scission of individual micelle chains. This type of dramatic failure can manifest itself as instabilities in not just extensional flows, but complex flows as well. For example, the flow around a sphere contains regions of shear as the fluid passes around the circumference, as well as extension in the wake of the sphere. Given that the fluid is known to be shear thinning as well as extensionally thickening, the combination of these qualities and the complex flow field yields some interesting results. Chen and Rothstein [15] observed that above a critical Deborah number a new class of elastic instabilities, related to the rupture of these micellar solutions in the extensional flow present in the wake of a sphere occurred. By measuring the flow fields with Particle Image Velocimetry (PIV) and Flow Induced Birefringence (FIB) they were able to explore the kinematics of the flow. Similar instabilities have also been observed by Gladden and Belmonte [16]. A natural extension of this work is to study the flow of viscoelastic micelle solutions past periodic arrays of cylinders.

Fluid flow around a single cylinder in cross-flow has also been the subject of much experimental treatment. One such study was performed by McKinley et al. [17] using Laser Doppler Velocimetry (LDV) to observe the behavior and flow patterns generated by several different polymer solutions flowing around a circular cylinder. They experimentally observed and verified the existence of a flow instability in the wake of a single cylinder lying perpendicular to the bulk flow above a critical Deborah number of $De_{crit} = 1.3$. The Deborah number is defined as $De = \lambda\dot{\gamma}$, where λ is the relaxation time of the fluid, and $\dot{\gamma}$ is the shear rate. In similar experiments of flow of polymer solutions past an array of cylinders at low Reynolds number, Chmielewski et al. [18] also observed an elastic instability. They found an enhanced pressure drop for all array configurations when the Deborah took on a value of order 1 as well as unsteady flow patterns. There are many other experimental studies in the canon of investigations into the flow of viscoelastic polymer solutions around a cylinder showing similar results including work from Talwar et al. [19], Baaijens et al. [20,21], Usui [22], Dhahir [23], Verhelst [24], Ogata [25] and others [26–28], however no experiments to date have investigated the flow of wormlike micelles past a single, or periodic array of cylinders.

In a numerical investigation of the flow of viscoelastic fluids past a cylinder, Hulsen et al. [29] used both Oldryod-B and Giesekus equations of state to observe the response of the drag coefficient to varying flow conditions. Over the range of Deborah numbers tested, they found that the dimensionless drag coefficient was a non-linear function of Deborah number. Their results show that the drag coefficient initially decreases with increasing Deborah number, then at a Deborah number of $De = 2$, it begins to increase, eventually growing larger than the Newtonian response. Liu et al. [26,27] performed a numerical study of the flow past a periodic array of cylinders using both Giesekus, FENE-P and FENE-CR constitutive models. They predicted similar non-linear trends in the drag as those predicted by Hulsen et al. [29]. Additionally, their results indicate that above a critical Deborah number, $De_{crit} \approx 1.5$, the drag coefficient becomes time variant. These results are relevant not only due to the parametric variation of inter-cylinder spacing, but parametric variation in constitutive models as well. They demonstrated that shear thinning can play a large role in the fluid dynamics and resulting drag especially when the containment effects of the channel are important.

Smith et al. [30] performed a linear stability analysis of the flow around an array of cylinders. They predicted an elastic instability for flows above a critical Deborah number, which depends on the spacing between cylinders in a continuous array. Moreover, they predict that the nature of the instability will transition from being shear to extensionally dominated as the inter-cylinder spacing is increased. More recently, Oilveira et al. [31] performed a numerical study employing a FENE-CR equation of state to investigate the nature of the instability in the wake of a cylinder. Their results show that in flows where the local Deborah number exceeds $De \geq 1.3$ a time dependant drag coefficient emerges. The periodic array of cylinders is an idealized porous medium which can be useful in gaining insight into the flow through membranes, rock beds etc.

The flow of viscoelastic solutions through porous media is a classically studied problem [26–28,32–34]. However, most of the viscoelastic studies performed thus far have used polymeric fluids. Understanding the flow of viscoelastic wormlike micelle solutions through porous media has become an extremely important industrial problem because wormlike micelle solutions are finding use in enhanced oil recovery where they are often used as a polymer-free fracture fluid for stimulating oil production [1,2,35,36]. Fracture fluids are driven into recovery wells at enormous pressure in order to open up cracks in the sandstone and speed up oil recovery. Wormlike micelle solutions are ideal for these applications because they shear thin extremely quickly which allows them to be pumped relatively easily and at low cost. Additionally, the high zero-shear viscosity of the fracture fluids allows sand or other proppants to be suspended in the fluid and transported to the newly induced fracture under pressure where they pack tightly enough to keep the fracture from fully closing when the well is depressurized, yet with enough permeability to maintain efficient flow. Wormlike micelle solutions have found use in a number of other oilfield applications as well. For a more complete and detailed review, the reader is directed to the papers by Maitland [35] and Kefi et al. [2]. The flow through porous media is a tortuous flow with regions of high shear in cracks and narrow capillaries and regions of strong extensional flow as the fluid is accelerated into capillaries from relatively large reservoirs or holes within the rock. Unfortunately, flow through cores of sandstone or other opaque porous media it is difficult to analyze because the exact nature of the media is unknown and the flow cannot be visualized. For that reason, most porous media studies use an idealized porous media like a packed bed of glass spheres where the permeability and tortuosity are known a priori and the flow can be observed to some extent with proper index of refraction matching [37,38] or in our case the flow through a periodic array of cylinders.

For Newtonian fluids in porous media, the flow can be described using Darcy's law which states that the average velocity through the media can be determined from $\bar{V} = \phi \Delta p/\mu$, where ϕ is the porosity of the media, Δp is the pressure drop and μ is the Newtonian viscosity [39]. Clearly, when the fluid is viscoelastic, Darcy's law is not sufficient to describe the flow rate as a function of pressure drop. Often, an effective Darcy's viscosity or a resistance coefficient, $\Delta = \mu_{app}/\mu$, are measured experimentally or derived through numerical simulations as a function of flow rate for viscoelastic fluids so that Darcy's law can continue to be used. For polymers like polyacrylamide (PAA) which strain harden in extensional flows and shear thin in shear flows, extremely large effective Darcy viscosities have been measured demonstrating how dominant the extensional component of porous media can be to the overall flow [37,40]. Similar observations were also made for wormlike micelle solutions [38,41]. Muller et al. [38] investigated the flow of a CTAT solution through a packed bed of monodisperse 1 mm glass spheres. The shear rheology of the CTAT showed a modest shear thickening while the opposed-jet measurements of the extensional viscosity showed very little if any strain hardening. Although, it should be noted that the lack of strain hardening might simply be a result of scission of the wormlike micelles at the very large extension rates applied. For relatively low CTAT concentrations, the resistance coefficient was found to increase quite dramatically with increasing shear rate. The increase is an order of magnitude larger than the shear thickening observed which the authors hypothesize is a synergistic interaction between the shear and extensional components of this complex flow resulting in the large observed viscosity enhancement [38]. Further, Rojas et al. [42] recently explored the relation between the shear rheology of micellar solutions and the enhanced flow resistance in porous media. That body of work was conducted at relatively high Reynolds number, but indicated a dramatic interplay between the shear thickening behavior of the fluid and the measured pressure drop. Similar behavior was observed even for the most dilute solutions that the authors explored even those not demonstrating shear thickening. Recently, Boek et al. [43] experimentally investigated the flow of EHAC through a micro fluidic expansion contraction. Micro particle image velocimetry (μ-PIV) measurements of the flow through this idealized pore showed large recirculation regions upstream of the contraction. As has been seen with similar flows of polymer solutions [44,45], these vortices appeared to be unstable thus demonstrating how complex the flow through the pore space in natural rock can be.

The outline of this paper is as follows. In Section 2, we briefly describe the experimental setup, the implementation of several measurement techniques including flow induced birefringence and particle image velocimetry and the shear and extensional rheology of the wormlike micelle solutions used. In Section 3 we discuss the experimental results and in Section 4 we conclude.

2. Experimental details

2.1. Flow geometry and experimental setup

A schematic diagram of the test geometry can be seen in Fig. 2. The circular cylinders that serve as the two by three periodic array were fabricated from acrylic rod, and precisely lathed down to a uniform diameter of $D = 10$ mm. The machined cylinders were mounted transversally in a rectangular channel with a cross sectional area of 46.3 mm × 66.6 mm, measuring 340 mm in length. This arrangement leads to an effective blockage ratio of 30%, and a diameter to channel height of 6.5:1. In order to avoid containment effects, the periodic array was placed such that a cylinder to channel width of at least 5:1 can be maintained. In this way, the greatest shear gradient experienced by the test fluid will be around the cylinder array and not the bounding channel walls. We thus define the nominal local Deborah number

$$De = \lambda \dot{\gamma} = \lambda \frac{U}{R}. \quad (1)$$

where λ is the characteristic fluid relaxation time (representative temperature adjusted values can be found in Table 1), R is the radius of a single cylinder in the periodic array and U is the mass averaged

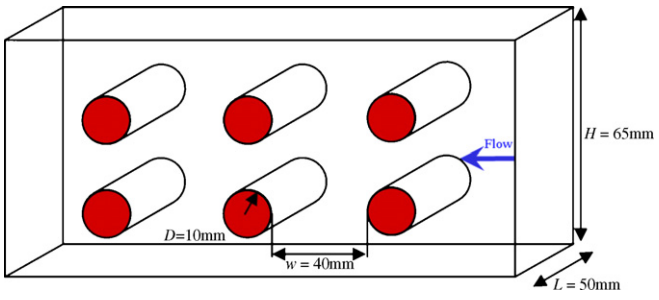

Fig. 2. Schematic diagram of periodic array of cylinders experimental flow cell.

Table 1
Parameters characterizing the rheology of the wormlike micelle solutions at $T = 25\,^{\circ}C$.

	CPyCl–NaSal (100 mM/50 mM)	CTAB–NaSal (50 mM/50 mM)
Zero-shear viscosity, η_0 (Pa s)	11	65
Plateau modulus, G_0 (Pa)	27	12
Relaxation time, λ (s)	0.50	5.3

velocity in the bulk flow about the periodic array. To minimize the driving pressure fluctuations, a positive displacement piston pump was fabricated and used to produce a precisely controllable, constant flow rate through the channel. The piston motion was controlled with addressable micro-staging, capable of a flow rate resolution of $4\,mm^3/s$. Due to the precision of the pumping system, the Deborah number can be accurately controlled, allowing for a repeatable and accurate interrogation of the test fluid using any number of measurement techniques. In this study, a range of Deborah numbers $0.1 \leq De \leq 10$, corresponding to flow rates of $(2.25 \leq Q \leq 225\,cm^3/s)$ was probed to explore the pressure drop, flow kinematics, and flow induced birefringence as a function of Deborah number and test fluid. The range of Deborah numbers was limited at the high end by the capacity of the system and thus the measurement time available for the artifacts of the experimental set-up to die out.

In order to measure the fluid's behavior, the flow cell was constructed with pressure taps machined into the bounding side plates. Solutions of viscoelastic fluids have been shown to be very sensitive to recirculation within tap holes. Accordingly, the pressure taps were mounted flush with the walls and covered with a fine mesh in order to minimize this effect. Pressure lines were then plumbed from the taps into a differential pressure transducer (Omega PX154010-DI). The signal from the pressure transducer was fed into a data acquisition board and sampled at 100 Hz using Labview software.

2.2. Particle image velocimetry

In order to quantitatively measure the velocity fields through the array of cylinders, the fluid was seeded with reflective glass micro-spheres (Potter Industries Sphericell) at 0.005% by weight, and allowed to equilibrate in the test geometry for 24 h. The seeded fluid was then illuminated using a laser light sheet generated by a monochromatic Argon laser source (National Laser 500 mW 450–515 nm). The lens and fiber optical train used produced a window of near uniform illumination approximately 75 mm in length and 0.2 mm in width, allowing for velocity profile measurements over the full channel height. Upon illumination, the fluorescent spheres' motion was captured with a high speed camera (Phantom v #5.1) at 100 fps, and broken into a sequence of digital images using Phantom's control software. The image sequence was then processed using LaVision's Particle Image Velocimetry (PIV) software. The resulting vector fields were then further analyzed in order to gain insight into the regions showing potentially interesting flow phenomenon. In the case of the CPyCl–NaSal test fluid, the flow was stable at all flow rates tested, and the entire set of 150 computed vector fields could be statistically averaged to give a single clean ensemble mean vector field. However, the CTAB–NaSal test fluid showed some fluctuation in all measurement techniques at Deborah numbers greater than $De > 4.5$, thus fewer frames could be averaged together to obtain the time dependant velocity profiles. Therefore, while the same averaging protocol was used to highlight temporal and spatially averaged differences between the two fluids, it should be noted that this in does not imply an instantaneous resemblance of the test fluids at higher Deborah numbers.

In order to capture any deviations from Newtonian flow generated by the fluids elasticity, digital flow visualization was realized with the use of DaVis' image statistics functions. The ability to perform image summing, averaging and root mean square averaging, in a digital format allows for repeatable and efficient generation of stream- and streak-line photography. Since the test fluid was already seeded and illuminated to realize particle tracking, the particle's tracks could be recorded frame by frame to generate a composite path history image of the ensemble of illuminated spheres. By looking for streamline crossing and interaction, it is easy to see any discrepancy between the images captured and those expected for vanishingly small Reynolds number creeping flow. Additionally, they prove useful to compare to other studies of polymeric solutions through arrays of cylinders [46]. Specifically, Chmielewski et al. [18] have published a study of fluids in crossflow past arrays of cylinders, visualized by streakline imagery.

2.3. Flow induced birefringence (FIB)

The refractive index of a wormlike micelle varies depending on whether the light passes parallel or normal to the micelle's backbone. By passing light of a known polarization state and frequency through a fluid sample and measuring the resulting change in polarization state, flow-induced birefringence takes advantage of this fact to measure the deformation of the micelle. Under all flow conditions, this technique can at least qualitatively elucidate the regions of large stress in a flow. In the limit of small deformations, an optical train can be built up using Mueller calculus, and a value of the micellar deformation can be calculated from a stress-optic coefficient. Flow-induced birefringence measurements have been used quite extensively to examine both steady and transient flows of and wormlike micelles [11,15,47–49]. Flow-induced birefringence can be used to determine the local anisotropy in the conformation of the wormlike micelles $\Delta A = A_{11} - A_{22}$ [47]

$$\frac{\Delta n' \cos 2\chi}{C} = G_0 \Delta A, \tag{2}$$

where $\Delta n'$ is the measured birefringence, x is the extinction angle, C is the *stress-optical coefficient*, and G_0 is the plateau elastic modulus of the fluid. If the stress-optic rule holds, then the right hand side of Eq. (2) can be rewritten as the stress within the wormlike micelle.

To obtain full field flow induced birefringence measurements of the flow through the array of cylinders, the Osaki method was used. In order to acquire information about both the retardation and the extinction angle, the Osaka method requires flow induced birefringence measurements from two different crossed polarizer arrangements [47]. A monochromatic light source was used to illuminate the flow between crossed polarizers. A Nikon D70 digital camera was used to capture the birefringent patterns in the wormlike micelle solution generated by the flow for each linear polarizer configuration. The images were then processed using a Matlab routine to determine the spatially averaged retardation and extinction angle of the wormlike micelle solutions. To achieve a quantitative measure of the retardation, the background signal of the CCD camera was first subtracted from each image and the intensity was normalized with the light intensity in the absence of the linear polarizers to generate the following two normalized intensities.

$$\begin{aligned} i_{0^\circ} &= \frac{2I_{0^\circ}}{I_{0,0^\circ}} = \sin^2(2\bar{\chi}) \sin^2\left(\frac{\bar{\delta}}{2}\right), \\ i_{45^\circ} &= \frac{2I_{45^\circ}}{I_{0,45^\circ}} = \cos^2(2\bar{\chi}) \sin^2\left(\frac{\bar{\delta}}{2}\right). \end{aligned} \tag{3}$$

where the i_{0° intensity is sensitive to deformations due to shear where $\bar{\chi} \cong 45^\circ$, and i_{45° is sensitive to deformations due to extensional flow where $\bar{\chi} \cong 0^\circ$. These two intensities were then

manipulated to generate a full field description of the spatially averaged values of the retardation and the extinction angle

$$\bar{\delta} = \frac{2\pi\Delta n' d}{\lambda_{light}} = \sin^{-1}\sqrt{i_{0^\circ} + i_{45^\circ}},$$
$$\bar{\chi} = \frac{1}{2}\tan^{-1}\sqrt{\frac{i_{0^\circ}}{i_{45^\circ}}}. \quad (4)$$

where d is the optical pathlength of the light, λ_{light} is the wavelength of the laser light. Note that the sign of the retardation and extinction angle calculated using the Osaki method is ambiguous. The resolution of this full field technique is limited by the camera to about $\delta \approx 0.1$ rad. Due to the extreme deformation the micellar network undergoes at high Deborah numbers, data analysis becomes impractical because the birefringence quickly goes through orders. Further, under the large stresses and deformation rates experienced, the linear relation in the stress-optic rule is no longer valid. As such, for the purpose of this study, the full field FIB technique is used only qualitatively to highlight the deformation; it is a visualization tool to aid the observer.

2.4. Fluid rheology

2.4.1. Sample preparation

Wormlike micelle solutions assembled from two different surfactant/salt combinations were chosen for this study. The first set of wormlike micelle solutions that were tested were made up 100 mM of the cationic surfactant cetylpyridinium chloride (CPyCl) (Fisher Scientific) and 50 mM of sodium salicylate (NaSal) (Fisher Scientific) dissolved in a brine of 100 mM NaCl in distilled water. The addition of the salt helps screen the charges on the hydrophilic head groups of the surfactant making the resulting micelle more flexible [50]. The electrostatic screening of the salt has been observed to lower the critical micellar concentration (CMC) for CPyCl in aqueous NaCl of CMC = 0.9–0.12 mM [51]. CPyCl and NaSal were obtained in dry form from Fisher Scientific. The CPyCl was dissolved in brine on a hot plate with a magnetic stirring bar. During mixing, a moderately elevated temperature was applied to reduce viscosity and aid in uniform mixing. After the solutions were fully dissolved, approximately 20–30 min, they were allowed to settle at room temperature for at least 24 h before any experiments were performed to allow air bubbles introduced during mixing to rise out of solution.

The second test fluid was composed of 50 mM of another cationic surfactant CTAB (Fisher Scientific) and 50 mM of NaSal in deionized water. This solutions is well above the critical micelle concentration, which for CTAB in pure water is CMC = 0.9 mM and is again significantly lower in the presence of salt [4]. The solution was prepared in the manner described above. At the concentrations used, the wormlike micelle solution is concentrated and entangled with significant number of entanglement points per chain [4].

When analyzing and presenting the experimental data, the relaxation times and viscosities were adjusted to their values at a reference temperature of $T_{ref} = 25\,^\circ$C using time-temperature superposition with a shift factor, a_T, defined by the Arrhenius equation [52]. Within the temperature range or our experiments, the Arrhenius form of the time–temperature superposition shift factor was found to be in good agreement with the rheological data for each of the wormlike micelle solutions tested, however, because of the sensitivity of the underlying wormlike micelle structure to temperature, every effort was made to maintain the fluid temperature to within plus or minus a few tenths of a degree for all of the experiments presented herein.

2.4.2. Shear rheology

The steady and dynamic shear rheology of the test fluids were characterized using a stress-controlled rheometer (TA instruments, AR2000) with a 6 cm/2° cone-and-plate geometry. The micelle solutions were loaded and allowed to equilibrate for several minutes. The samples were not pre-sheared. In Fig. 3, the storage modulus, G', and loss modulus, G'', of the CPyCl–NaSal and the CTAB–NaSal wormlike micelle solutions are plotted as a function of angular frequency, ω. The viscoelastic properties of the fluids including zero shear rate viscosity, η_0, Maxwell relaxation time, λ and the elastic plateau modulus, G_N^0, are listed in Table 1. The deviation of the rheological data from the predictions of the single mode Maxwell model observed at large angular frequencies in Fig. 3 correspond to the Rouse-like behavior of the micelle between entanglement points [53] and can be used to determine both the breakup time, λ_{br}, and the reptation time, λ_{rep}, of the wormlike micelle chains. In the fast breaking limit $\lambda_{rep} \ll \lambda_{br}$, Cates showed that the breakup and reptation time could be related to the measured value of the Maxwell relaxation time through $\lambda = (\lambda_{rep}\lambda_{br})^{1/2}$ [54]. Additionally, the theoretical mesh size $\zeta_m = (KT/G_0)_{1/3}$ [55,56] can be determined in order to gain some information about the proximity of entanglement points and the density of the wormlike micelle mesh.

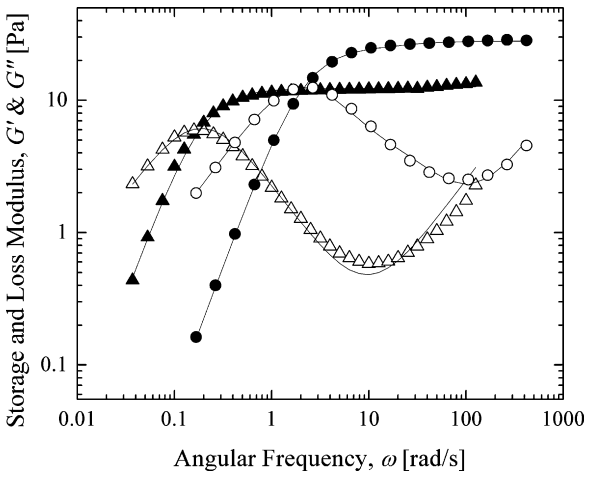

Fig. 3. Small amplitude oscillatory shear rheology of both CPyCl–NaSal solution in 100 mM NaCl '●' and CTAB–NaSal solution '▲' at $T = 25\,^\circ$C. The data in includes: storage modulus, G' (filled symbols), and loss modulus, G'' (open symbols), along with a two-mode Maxwell model fit for each fluid (—).

In Fig. 4, the steady shear viscosity, η, is plotted as a function of shear rate, $\dot{\gamma}$. At small shear rates and angular frequencies, the micelle solutions have a constant zero shear rate viscosity. As the shear rate is increased, the fluid begins to shear thin. At a critical

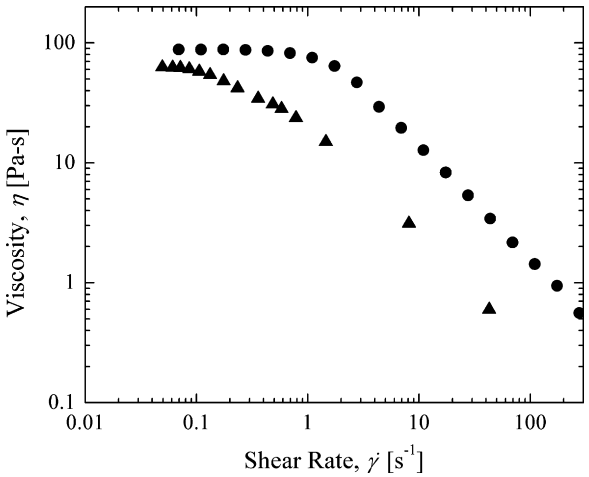

Fig. 4. Steady shear viscosity of both the CPyCl–NaSal solution '●' and the CTAB–NaSal solution '▲' at $T = 25\,^\circ$C.

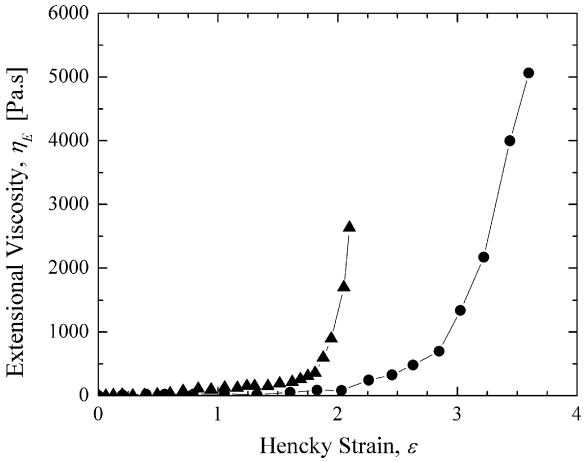

Fig. 5. The extensional viscosity as a function total strain for the 50/50 mM CTAB–NaSal wormlike micelle solution '▲' and the 100/50 mM CPyCl–NaSal wormlike micelle solution '●', stretched at a Deborah number of $De_{ext} = 1.3$, The experiments both end with the rupture of the fluid filament before a steady-state extensional viscosity could be reached.

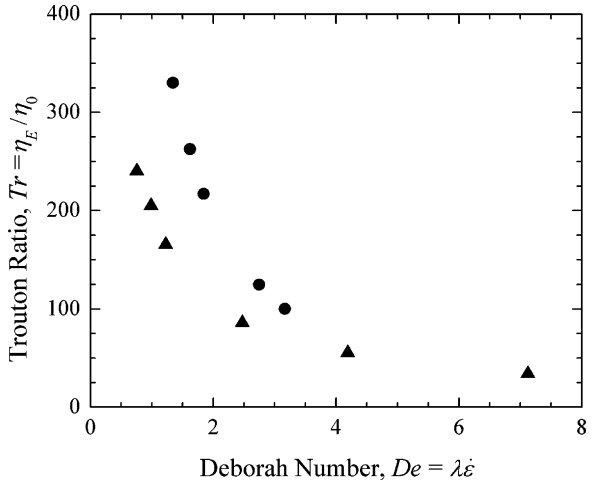

Fig. 6. Trouton ratio as a function of extensional Deborah number for both the 100/50 mM CPyCl–NaSal solution '●', and the 50/50 mM CTAB–NaSal solution '▲'.

shear rate, the viscosity drops precipitously approaching a slope of $\eta \propto \dot{\gamma}^{-1}$. For the CPyCl–NaSal solution, this plateau in the shear stress corresponds to the formation of two or more distinct shear bands. These shear bands have been recently measured and analyzed in our lab using particle image velocimetry (PIV) and flow induced birefringence (FIB) measurements and a specially designed large Couette flow cell [12]. The critical shear Deborah number for the onset of shear banding was found to be $De_{crit} = 2.0$ for the 100/50 mM CPyCl–NaSal solution. Although, we have not yet attempted to observe shear-banding in the CTAB–NaSal solutions, it could also account for the dramatic reduction in the shear viscosity observed in these systems and has been observed in the past for other CTAB solutions [57–59]. For the data presented in Fig. 4, a critical shear Deborah number of about $De_{crit} = 3.5$ is suggested for onset of shear banding in the 50/50 mM CTAB–NaSal solutions.

2.4.3. Extensional rheology

These particular solutions of wormlike micelles have been the subject of many experiments in extensional flow in recent years. Most recently, Rothstein et al. [60] have studied the effects of pre-shear on the extensional viscosity of solutions of varying concentrations. A filament stretching extensional rheometer (FiSER) capable of imposing a homogeneous uniaxial extension rate, $\dot{\varepsilon}$, on a fluid filament placed between its two endplates was used to make simultaneously measurements of the evolution in the force and the midpoint radius, R_{mid}. The transient extensional viscosity, η_E^+, may be extracted from the principle elastic tensile stress and is often non-dimensionalized as a Trouton ratio $Tr = \langle \tau_{zz} - \tau_{rr} \rangle / \eta_0 \dot{\varepsilon} = \eta_E^+ / \eta_0$. The deformation imposed upon the fluid filament can be described in terms of a Hencky strain, $\varepsilon = -2 \ln(R_{mid}/R_0)$ where R_0 is the initial midpoint radius of the fluid filament. The strength of the extensional flow is characterized by the Deborah number, $De_{ext} = \lambda\dot{\varepsilon}$ where λ is the relaxation time of the fluid and $\dot{\varepsilon}$ is the extensional rate. For a detailed description of the extensional rheometer used in these experiments see Rothstein [13].

The extensional rheology of the solutions tested have been previously investigated and published by Bhardwaj et al. [14,60] and Rothstein [13]. However, for completeness and for the purposes of direct comparison between the two wormlike micelle solutions tested, a representative set of extensional rheology data is reproduced here in Figs. 5 and 6. In Fig. 5 the extensional viscosity of the 50/50 mM CTAB–NaSal and 100/50 mM CPyCl–NaSal wormlike micelle solutions are plotted as a function total strain for similar Deborah numbers of $De = 1.3$, which we will show approximates the extension rates experienced by the fluid in the wake of the cylinders for the CTAB–NaSal solutions at the onset of an elastic instability. The extensional viscosity of both fluids was found to increase monotonically with increasing Hencky strain and demonstrate reasonably strong strain hardening with final Trouton ratios of $Tr = 165$ and 330 for the CTAB–NaSal and CPyCl–NaSal solutions respectively. The CPyCl–NaSal solution was consistently found to strain harden more than the CTAB–NaSal solution, however, the CTAB–NaSal solution strain hardened much more quickly, achieving maximum extensional viscosity at $\varepsilon \cong 2.0$, as opposed to $\varepsilon \cong 3.5$. At large extension rates, $De \gg 1$, the fluid filaments were all found to rupture. For all of the experiments that ended with a filament rupture, the final maximum elastic stress that was achieved in the fluid filaments of each solution was found to be constant independent of extension rate [14]. It has been hypothesized that the tensile stress of rupture corresponds to the maximum stress that the micelles can withstand before they begin to fail en masse [13]. For the 100/50 mM CPyCl–NaSal solutions the tensile stress at rupture was found to be $\Delta\tau_E \cong 7100$ Pa while for the CTAB–NaSal solution tensile stress at rupture was found to be lower at about $\Delta\tau_E \cong 2500$ Pa. The dynamics of the filament rupture have been captured with high-speed photography in the past and the interested reader is referred to Chen and Rothstein [15] or Bhardwaj et al. [14] for details.

In Fig. 6 the maximum Trouton ratio measured before filament rupture is plotted as a function of Deborah number. All of the experiments presented in Fig. 6 correspond to stretches which ended with a filament rupture. Owing to the constant elastic tensile stress achieved at rupture for the high Deborah number experiments, the maximum extensional viscosity achieved prior to rupture is found to decrease linearly with increasing imposed extension rate, $\eta_E \propto \dot{\varepsilon}^{-1}$. As seen previously in Fig. 5, one observes that the Trouton ratio of the CPyCl–NaSal solution is consistently larger than that of the CTAB–NaSal solutions. We will see in the following sections that the differences in the extensional rheology of these two wormlike micellar solutions have a significant effect on the response of the fluids as they flow through a periodic array of circular cylinders.

3. Results

3.1. Pressure drop

By measuring the pressure drop across the array of cylinders as a function of Deborah number and micellar solution, several

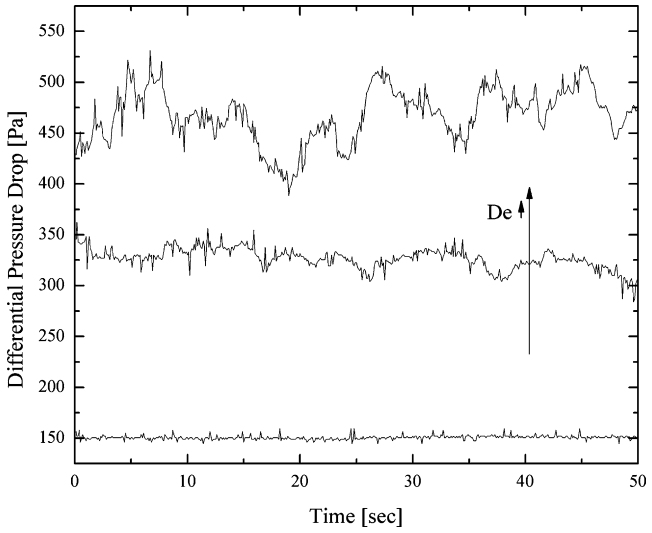

Fig. 7. Time transient pressure signals from differential pressure transducer during controlled mass flow rate experiment of the CTAB–NaSal solution. Increasing Deborah number flows appear sequentially higher, in order from bottom to top, $De = 0.5$, $De = 4.5$, $De = 10$.

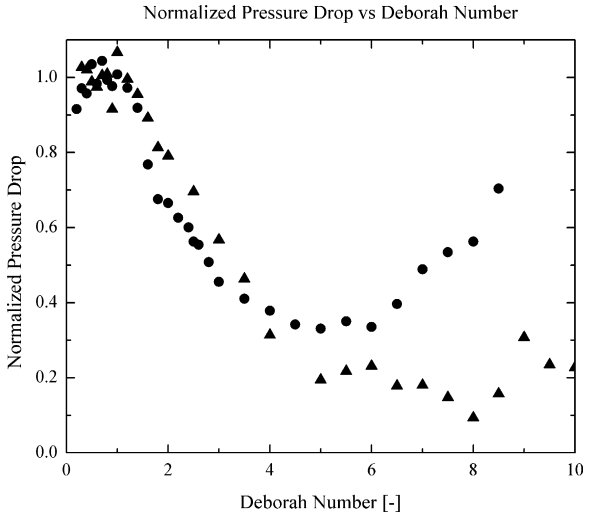

Fig. 8. Normalized pressure drop as a function of Deborah number for both test fluids , (▲) CTAB–NaSal solution, and (●) CPyCl–NaSal solution.

interesting phenomenon present themselves. In the case of the CTAB–NaSal, the characteristic of the transient response of the fluid varies as the Deborah number is increased. Above a critical Deborah number of $De_{crit} \approx 4.5$, the pressure drop response becomes temporally periodic, with the magnitude of the fluctuations increasing with increasing Deborah number. In Fig. 7 the effect of increasing Deborah number on the character of these transients is shown. At low Deborah numbers, the transient pressure drop signal is seen to remain nearly constant, with no long-time fluctuations. It is apparent that increasing the Deborah number qualitatively changes the response for $De > 4.5$. Thereafter, the signal exhibits sharp spikes. These spikes appear to be chaotic, exhibiting both high frequency deviations as well as longer-term dominant low frequency transients of roughly $f = 0.2$ Hz. Such chaotic fluctuations are not observed for the CPyCl–NaSal at any Deborah number, and remain approximately constant over the period of observation, typically on the order of hundreds of relaxation times.

In order to investigate the effects of the viscoelasticity of the wormlike micelle solution, the steady state value of the pressure drop was measured. The pressure drop, normalized by the response of a Newtonian fluid with the same zero shear viscosity, $\Pi \equiv \Delta P_{measured}/\Delta P_{Newtonian}$, was calculated from the time averaged pressure traces seen in Fig. 7 and is plotted in Fig. 8. Since no analytic solution for a Newtonian fluid through our flow geometry exists, the low-Deborah number pressure drop ($De \ll 1$), which increases linearly with increasing flow rate was used to approximate the Newtonian response. A line was fit to the low Deborah number pressure drop measurement curve, and used to normalize the entire range of Deborah numbers tested. The normalized pressure drop curve was found to exhibit four distinct regimes. In the low Deborah number regime, the normalized pressure drop is constant, corresponding to a normalized pressure drop of $\Pi \cong 1$. Although the zero-shear viscosities of the two solutions differ by a factor of approximately three, and the characteristic relaxation times differ by a factor of almost five, when the flow is cast in terms of Deborah number and pressure drop is measured at low Deborah numbers, the resulting plots collapse onto an apparent master curve, and are nearly identical. At a Deborah number greater than $De > 1$, where the bulk flow deforms the micelles faster than they can relax, a deviation in the pressure drop from a Newtonian response is observed. At moderate Deborah numbers ($1 < De < 4$), the normalized pressure drop decreases linearly with increasing Deborah number as a result of the shear thinning of the micelle solutions. As the flow rate is increased further ($4 < De < 7$), the normalized pressure drop levels out. In this regime, the solution is both shear thinning as well as extensional thickening and it would appear that the competition between the two effects roughly offset each other. Thereafter, a sharp upturn in the normalized pressure drop is observed with increasing Deborah number for the CPyCl–NaSal solution, but not for the CTAB–NaSal solution. This upturn in the pressure drop, as will become more apparent in the FIB measurements, is due to the onset of thickening of the extensional viscosity of the CPyCl–NaSal solution. However, before significant hardening of the CTAB–NaSal solution could occur, the onset of a flow instability was observed at a Deborah number of $De = 4.5$. The CPyCl–NaSal solutions were found to remain stable for all the experiments presented here.

The trends in the pressure drop data and the form on the instability match well with a recent study of the drag correction factor on a sphere falling through a solution of wormlike micelles performed by Chen and Rothstein [15]. These trends also match very well with recent observations by Talwar et al. [19] who studied the flow of polymer solutions through periodic arrays of cylinders as well as others [17,19,24,26,27,46,61–63]. They reported a dimensionless drag in terms of the product of the friction factor and the Reynolds number fRe. At low Reynolds number they found fRe to remain constant at $fRe = 1$. At moderate Reynolds numbers, the drag decreased before trending upward with further increase in Reynolds number. These results are in good qualitative agreement with the pressure drop trends seen in Fig. 8 for the CPyCl–NaSal solution. This observed upturn occurred at Reynolds numbers that were not vanishingly small, but were small enough that the effects of inertia were negligible. Similar observations of non-linear drag have also been reported by Liu et al. [27]. By investigating the effect of the finite extensibility parameter in the FENE-CR model, they went on to show that the upturn in the drag is likely the result of large extensional deformations of the fluid in the wake of the circular cylinders. In the channel geometry used by Liu et al. [27] confinement effects were present. They comment that these confinement effects serve to couple the shear-thinning and extensional properties of the fluid. Although the highest shear rate in out flow geometry occurs around the cylinder, the confining walls can cause the fluid to be sheared prior to flowing around the cylinders in the periodic array. As such, the interaction of the shear-thinned fluid with the extensionally hardened fluid may well explain the trends in pressure drop. The extensional rheology measurements of Bhardwaj et al. [60] showed

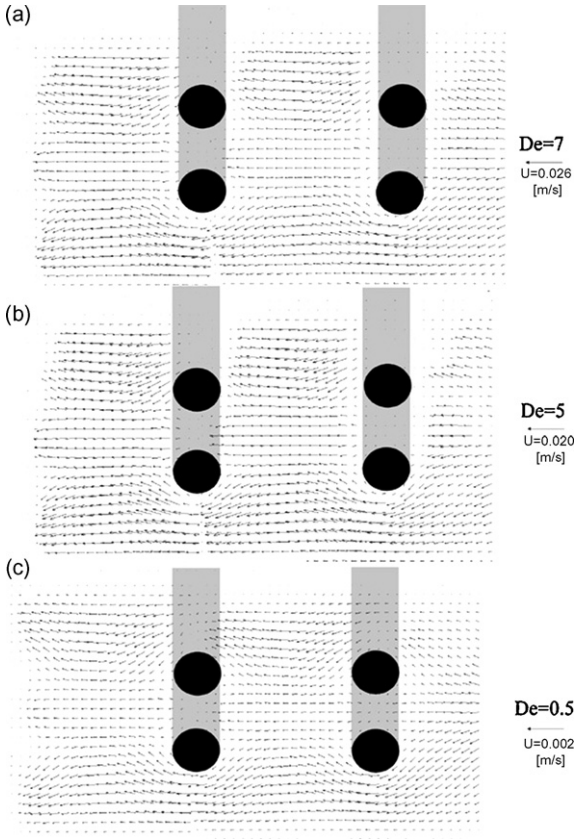

Fig. 9. Composite time averaged PIV vector fields for CPyCl–NaSal solution.

that wormlike micellar solutions are very susceptible to the effect of pre-shear. They found that pre-shear forestalls strain hardening to larger Hencky strains and reduces the critical stress for filament rupture. In our geometry the shearing might therefore reduce the effect of strain hardening and increase the susceptibility of these fluids to elastic instabilities resulting from the breakdown of those wormlike micelle solutions in the strong extensional flow present in the wake of the circular cylinders. These findings are in good agreement with Chmielewski et al. [64] who also found the flows of polymer solutions past cylinders to be unstable above a critical Deborah number.

3.2. Particle image velocimetry (PIV)

Velocity vector fields were constructed using particle image velocimetry (PIV) for each representative regime of the pressure drop parameter space and each test fluid. These velocity fields are presented in Fig. 9. As with the pressure drop results, the vector fields are similar at comparable Deborah numbers less than $De < 1$, before the effects of the fluid's elasticity become important. However, at moderate to large Deborah numbers, the elastic effects dominate resulting in interesting flow phenomenon. At low Deborah numbers, both micellar solutions exhibit nearly perfect fore-aft symmetry about all of the cylinders. In this regime, the magnitude of the velocity vectors scale linearly with Deborah number. Additionally, because both fluids behave as Newtonian in this regime, no apparent differences in the vector fields are observable between the two micellar solutions. As the Deborah number is increased, the shear thinning effects of the two fluids dominate, and deviations from the Newtonian regime become apparent. Comparing Fig. 9b and c it can be seen that at higher Deborah numbers, the velocity vectors are no longer mirror symmetric about a plane halfway between successive cylinders. In the case of the CPyCl–NaSal solution, velocity vector fields become more anti-symmetric as it flows around each subsequent set of cylinders. Larger velocity gradients are observed downstream as additional previously sheared and deformed fluid interacts and is swept into the bulk flow before it has had a chance to relax back to a stress equilibrium state. In the case of the CTAB–NaSal solution, the deviations from symmetry are manifest in an enhancement of the low velocity extensional flow in the wake of the cylinders, and a resulting velocity gradient increase in the spanwise direction. These gradients increase with increasing Deborah number, as observed in Fig. 9a–c which show measured Deborah numbers of $De = 0.5$, $De = 5$ and $De = 7$ respectively. As these velocity gradients increase, the shear thinning and strain hardening effects become more prominent.

At large Deborah numbers, $De \geq 4.5$, the CPyCl–NaSal solutions are stable and the pressure drop increases with increasing Deborah number. At these large Deborah numbers, the CTAB–NaSal solutions become unstable. As the fluid is sheared by passing around the cylinders, and then stretched in the wake, large elastic stresses are built up in both fluids. This effect can be seen explicitly in the FIB measurements presented in the next section. Under the strong flows present at higher Deborah numbers, the velocity vectors of the CTAB–NaSal solutions begin to show large deviations from the bulk flow, as the flow becomes temporally unstable. This effect can clearly be seen in the PIV results where the vectors oscillate back and forth at a frequency of approximately $f \approx 0.66$ Hz.

Presented in Fig. 10 are a series of three PIV computed vector fields, each at equal time spacing ($\Delta t = 0.66$ s). It can be seen that over a period of 1.5 s, the vectors complete one full cycle of dominance in the $+y$ to $-y$ directions. This frequency of oscillation roughly matches the dominant frequency found by taking the Fourier Transform of the transient pressure drop data, though no further correlation between Deborah number and dominant frequency was found. In order to further explore the nature of this instability in the CTAB–NaSal fluid, streakline images are presented in Fig. 11, wherein the streaklines at high Deborah numbers, $De = 10$, cross and exhibit what appears to be elastic recoil. Such images follow the work of Chmielewski et al. [18], who reported an elastic instability in the crossflow of polyisobutylene solutions through periodic geometries. They found that their Boger fluids began to exhibit asymmetric streamlines above a critical Deborah number of $De_{crit} = 1.5$ for one configuration and $De_{crit} = 0.5$ for the other even though the Reynolds number was negligible. It should be noted that the velocity fluctuations observed my Chmielewski et al. [18] were significantly smaller than those observed here and were confined to a region in close proximity to the trailing edge of the cylinder. The instabilities observed herein appear to affect the flow globally and do not have a well defined periodic nature even very close to the critical Deborah for onset. These observations suggest that this instability may not be the same elastic instability observed in the flow of polymer solution, but might stem from the breakdown of wormlike micelle solutions under large stresses similar to that observed by Chen and Rothstein [15] during the sedimentation of a sphere. These stresses are continually built after the successive sets of cylinders whereby the fluid has a chance to sample regions of high shear as well as extension. As we will see in the subsequent section, these kinematic effects combine to generate large stresses in the micelle chains, which are known to fail in extensional flows above a critical value of stress.

By examining the plots of the shear and extensional rheology (Figs. 4 and 5) it becomes clear that the CTAB–NaSal solution shear thins to a lower viscosity than the CPyCl–NaSal and is less capable of supporting elastic tensile stresses before rupturing in extensional flows. It is instructive to use the calculated PIV vector fields to map out where the flow field lies in the rheological space of the two fluids. The local extension rate, $\dot{\varepsilon}$, and shear rate, $\dot{\gamma}$, can be cal-

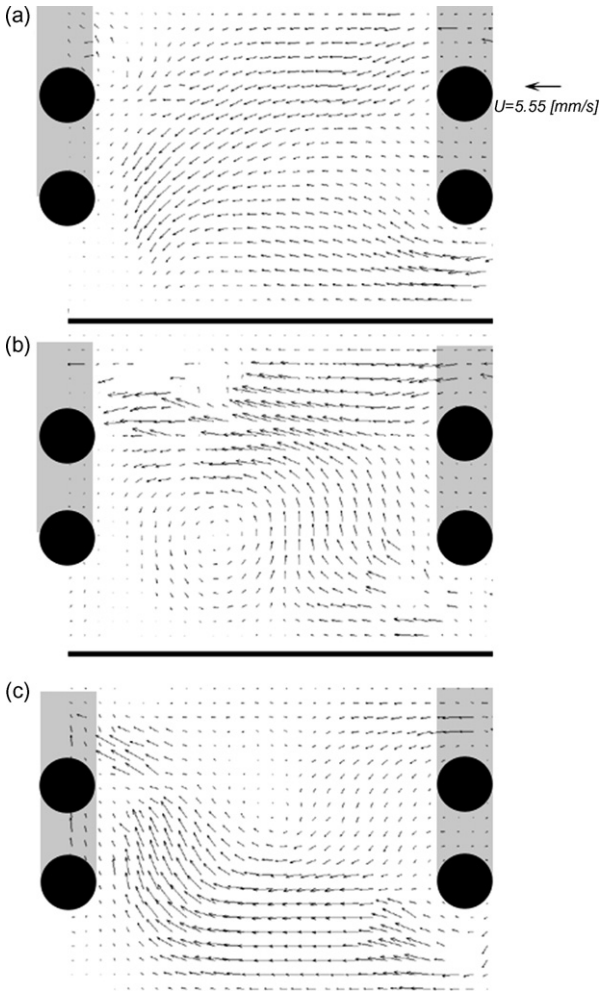

Fig. 10. Sequential PIV images highlighting unstable flow of the CTAB–NaSal solution at a Deborah number of $De = 10$. Each image represents a time step of 0.66 s.

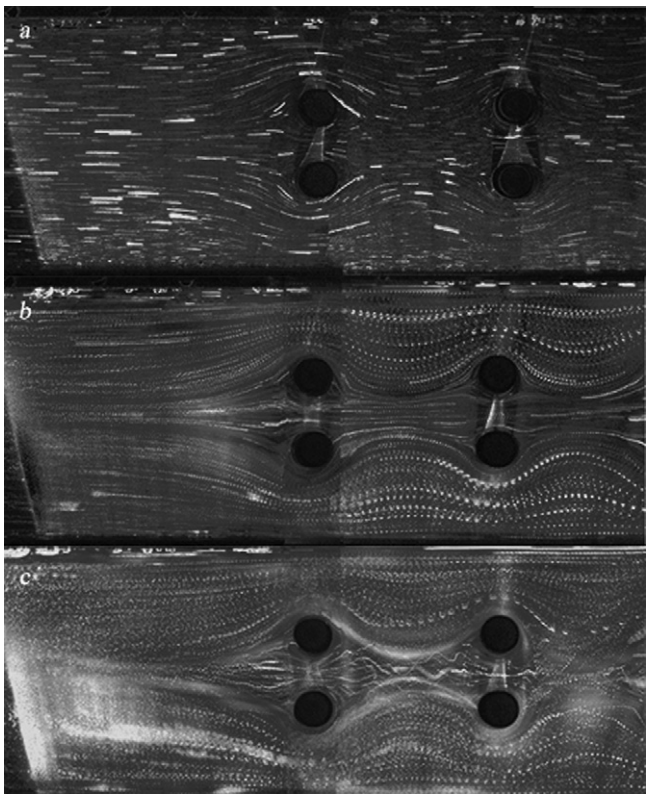

Fig. 11. Composite image of streaklines in CTAB–NaSal solution for Deborah numbers of $De = 0.5$ (a), $De = 5$ (b) and $De = 10$ (c).

culated by spatially differentiating the velocity profiles around the circular cylinders. Additionally, the accumulated extensional strain can be calculated by temporally integrating the extensional strain rates in key areas like between the circular cylinders and in their wake where extensional effects will dominate shear at large Deborah numbers. By doing so, trends in pressure drop and flow stability can be more closely compared to the shear and extensional rheology of each fluid. As the Deborah number is increased, the extension rate downstream of the circular cylinders is found to increase. However, the total strain experienced by a fluid element remains fixed at approximately $\varepsilon \approx 2.5$ over all Deborah numbers tested. The constant value of strain is due to the decrease in residence time as the Deborah number and extension rate are increased. These results are in good agreement with those reported by Chmielewski et al. [64] where they argue that in the wake of a cylinder, nominal strains of $\varepsilon = 3$ can be built up.

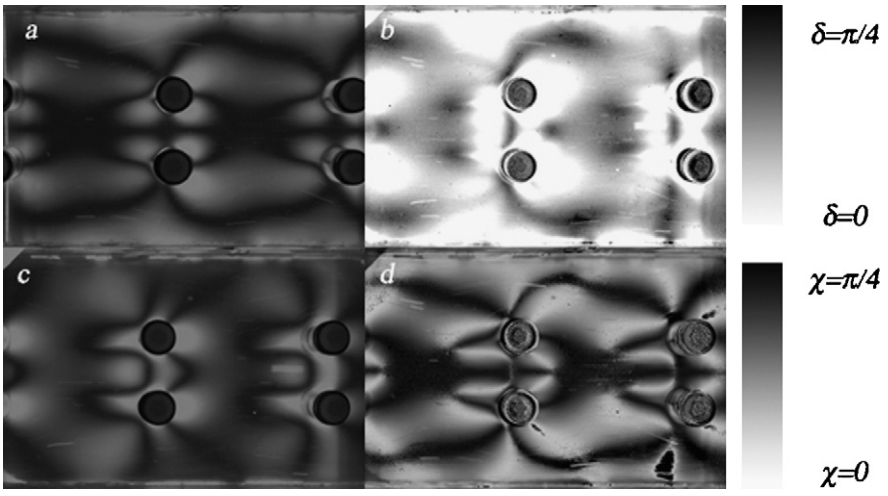

Fig. 12. FIB measurements of the CPyCl–NaSal test fluid flowing through the periodic array of cylinders. The measurements were taken at $De = 4$, and include polarizers aligned at 0° and 90° (a), cross polarizers aligned at 45° and 135° (c) , calculated x (d), and calculated δ (b).

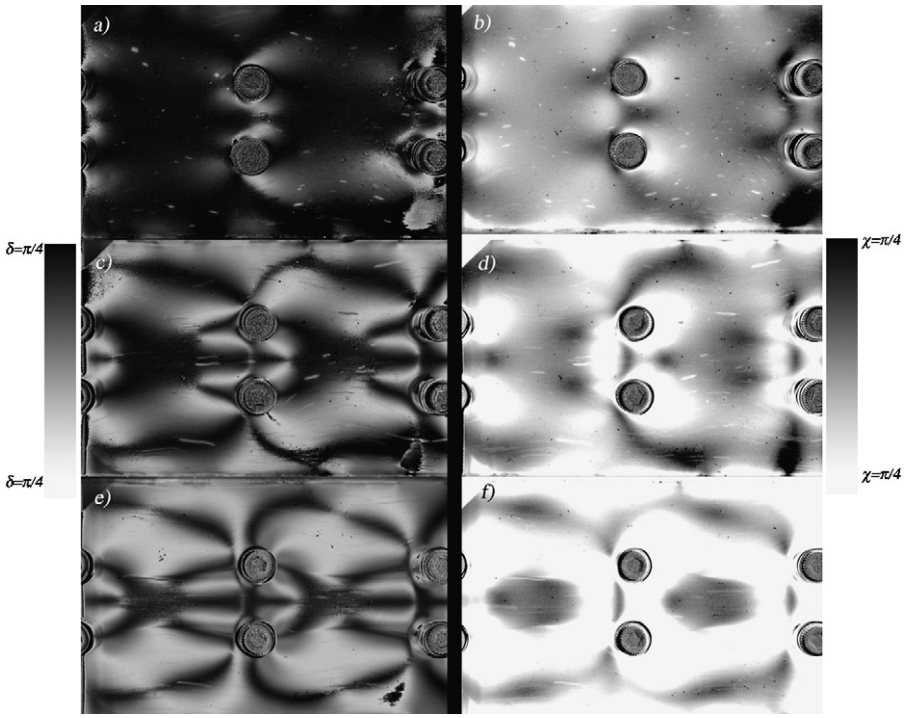

Fig. 13. FIB results showing δ (left) and x (right) for the CPyCl–NaSal test solution at Deborah numbers of $De = 1$ (a and b), $De = 3$ (c and d) and $De = 8$ (e and f).

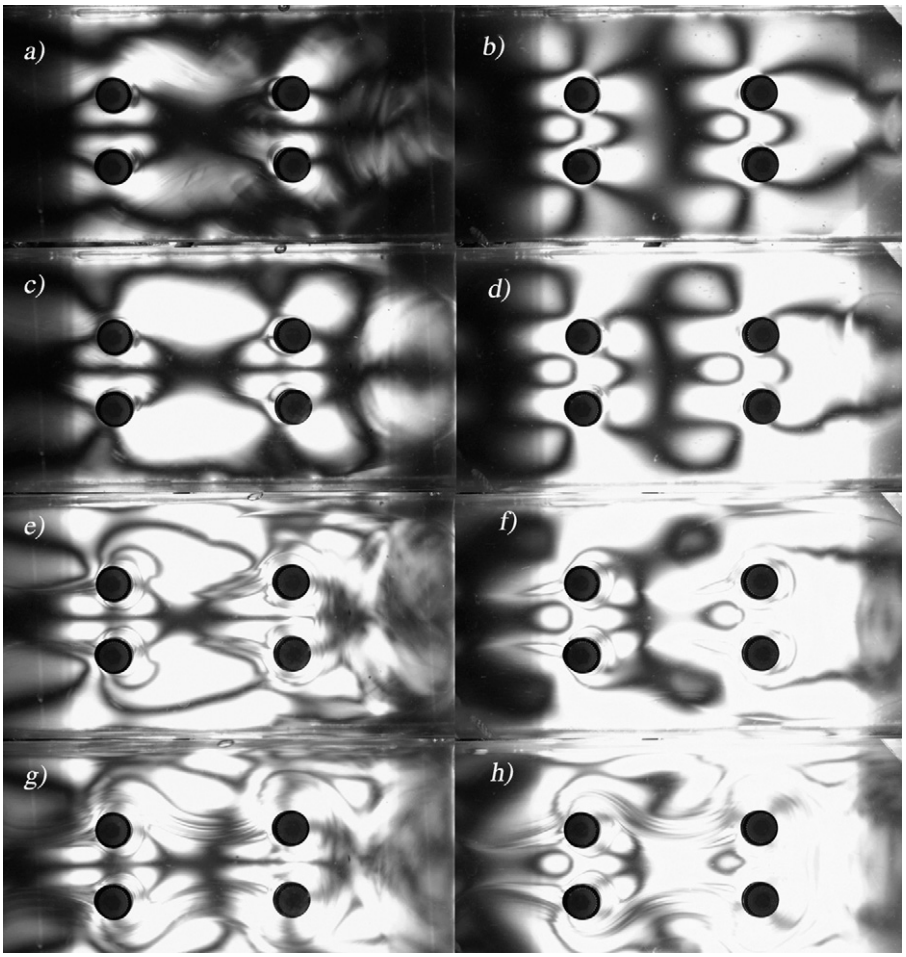

Fig. 14. FIB images for the CTAB–NaSal test fluid highlighting shear flow on the right column and extensional flow on the left at Deborah numbers of $De = 1$ (a and b), $De = 2$ (c and d), $De = 4$ (e and f) and $De = 8$ (g and h).

At a Deborah number of $De = 4.5$, where the CTAB–NaSal solutions become unstable an extension rate of $\dot{\varepsilon} = 0.21\,s^{-1}$, or equivalently at an extensional number of $De_{ext} = \lambda\dot{\varepsilon} = 1.2$, present in the wake of the cylinder. At this extension rate and a strain of $\varepsilon \approx 2.5$, the extensional rheology in Fig. 5 indicates that the CTAB–NaSal solutions will have built up enough extensional stress to rupture. This extensional flow induced failure of the wormlike micelle solution is likely the cause of the flow instability. Additionally, pre-shear of these wormlike micellar solutions prior to extension has been shown to result in filament rupture at a significantly smaller extensional stresses and accumulated strains, making micelle failure even more likely in the wake of the cylinders [60]. From Fig. 5, it can clearly be seen that the CPyCl–NaSal solution requires much more strain, or a significantly larger extension rate than the CTAB–NaSal to rupture. The upturn in the pressure drop for the CPyCl–NaSal solutions is thus linked to the extensional thickening that occurs at the rates without micelle failure. Even at a Deborah number of $De = 8$, the CPyCl–NaSal solutions experience an extension rate of $\dot{\varepsilon} = 1.75\,s^{-1}$ ($De_{ext} = 1.0$) and a strain of $\varepsilon \approx 2.5$ in the wake of the circular cylinder, which the extensional rheology in Fig. 5 shows that should not cause the micelle to rupture. This is evidence that the breakdown of the wormlike micelles in the strong extensional flow in the wake of the circular cylinder is likely the cause of the flow instability. If this was a purely elastic flow instability, one would expect these two fluids to become unstable at roughly the same Deborah number and mirror the results found in the literature for polymer solutions. It can therefore be concluded that the high Deborah number pressure drop measurements can be directly correlated to the extensional rheology of the two test solutions.

3.3. Flow induced birefringence

The Osaki crossed polarizer technique described in Section 2.3 was used to produce flow induced birefringence measurements at different Deborah numbers in each of the distinct flow regimes. At low Deborah numbers in the Newtonian response regime, where the flow field is spatially and temporally stable and reversible, identical conditions could be repeatably reproduced for both test solutions. This reproducibility allows for a complete FIB analysis using the Osaki method and Eqs. (2) and (3). The CPyCl–NaSal solution remains completely stable and reproducible for all Deborah numbers tested, allowing for a complete analysis, while the CTAB–NaSal solution exhibits an instability, making analysis difficult at higher Deborah numbers. The areas of large deformation for each orientation of the polarizers are clearly seen in Fig. 12. In the case of 0° and 90°, the regions of deformation due to shear appear as relatively light areas in Fig. 12a, and precisely where expected, at 45° normal to the bulk flow. This pattern is nearly the same for each proceeding cylinder as the fluid travels downstream. In the case of 45° and 135°, the regions of extensional deformation appear as bright areas directly in the wake of each cylinder, growing in length as the flow proceeds downstream as seen in Fig. 12c.

By using an image analysis algorithm, the values of the retardation, δ, and extinction, x, can be calculated from Eq. (4) and are presented in Fig. 12b and d respectively. By calculating these values and comparing the two test fluids, we see that at comparable Deborah numbers, the CTAB–NaSal is considerably more birefringent than the CPyCl–NaSal. Even taking into account the difference in the stress-optical coefficient ($C = 4.5 \times 10^{-7}\,Pa^{-1}$ for the CTAB–NaSal vs. $C = 3.1 \times 10^{-7}\,Pa^{-1}$ for the CPyCl–NaSal solution) [47] it is clear that the CTAB solution experiences considerably more deformation and stress. This is most clearly noticeable in comparing Figs. 13 and 14. It is readily apparent that the CPyCl–NaSal solution, shown in Fig. 13 exhibits stable birefringent patterns, which change little in form as the Deborah number is increased. The CTAB–NaSal on the other hand, shown in Fig. 14, experiences so much deformation that the birefringence quickly goes through orders, as the Deborah number is increased, making determination of the retardation angle difficult. More specifically, as seen in Fig. 14e due to increasing deformation of the micelles near the second set of cylinders the birefringent bands transition quickly from light to dark to light again. As such, only values of $i_{0°}$ and $i_{45°}$ are presented. Additionally, it is observed that the birefringent patterns change characteristics as the Deborah number is increased; the instability presents itself as large deformational deviations from the steady patterns observed in the CPyCl–NaSal solution. A bright, birefringent band in the extensional wake of the cylinder is seen to grow with increasing Deborah number. The length of this band increases until it reaches the next cylinder, at which point, it bends towards the centerline. This extensional deformation directly corresponds

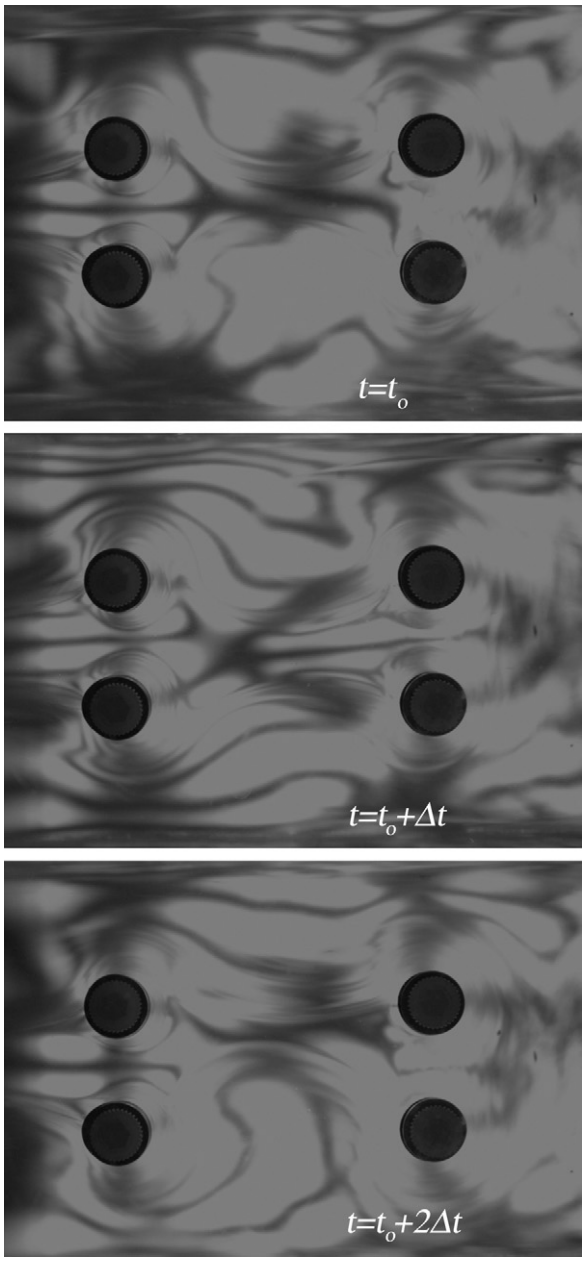

Fig. 15. FIB focusing on the unsteady deformation between the cylinders for the CTAB–NaSal test fluid at a Deborah number of $De = 6$. Here, cross polarizers are oriented at 0° and 90°. Local deformation and alignment appear as thin 'wispy' bands of light and dark. The images are separated by a $\Delta t = 1.0$ s.

to the enhanced necking seen in the PIV results of Fig. 9. Additionally, it can be seen that the number of orders the birefringence goes through appears to scale linearly with Deborah number; by doubling the Deborah number from two to four, the number of bands of light and dark seen in the extensional wake double. This observation is in good qualitative agreement with studies by Kim et al. [65] who report contours of constant stress and negative wake generation in a FENE-CR constitutive model. Although we are unable to calculate a value of stress, the patterns of observed birefringence match closely with the calculated contours of stress. Similar observations were recently reported by Afonso et al. [66] who studied the flow past a falling cylinder with several constitutive models. Their reported contours of normalized normal stress τ_{xx} with a FENE-CR model match the birefringence highlighting extensional flow, shown in Fig. 14 quite well.

In order to further capture the nature of the instability, a sequence of tight zoom photographs into the space between the cylinder array is presented in Fig. 15, with polarizers oriented at 0° and 90°, to emphasize the deformation due to shearing. It can be seen that the birefringent patterns are unstable, and undergo large scale changes of stress and thus micelle deformation. These changes fluctuate not only in direction, but number of bands, implying that structural order is being built up by the flow, and then broken down. This time sequence is representative of the periodic motion of the CTAB–NaSal micelles as they flow through the cylinder array at high Deborah numbers.

4. Conclusions

In this paper, we have presented the results of our investigation into the flow fields generated by two different solutions of wormlike micelles flowing through an idealized porous media: a periodic array of circular cylinders. By systematically varying the Deborah number, the flow kinematics, stability and pressure drop were measured and used to investigate the distinct differences in the response of two fluids to the cylinder array. The pressure drop was found to initially decrease due to the shear thinning of the test fluid, before increasing at large flow rates as extensional effects begin to dominate the flow. An elastic instability in one of the test fluids was observed above a critical Deborah number, while the other fluid was found to remain stable for the flow rates tested in our experiments. The kinematics of both fluids were fully investigated using PIV and FIB to elucidate the nature of the flow and the observed elastic instability. The disparity in the response of the two test fluids can be attributed to the measurable differences in their extensional rheology. At the Deborah numbers investigated in this study, the elastic instability and the resulting kinematics observed through PIV, FIB and pressure drop measurements were only observed in the CTAB–NaSal solution. Although the CTAB–NaSal shows strain hardening, and can exhibit large Trouton ratios, the CTAB–NaSal micellar network is incapable of supporting the same level of extensional stresses as the CPyCl–NaSal solution. The differences in the rheology of the two fluids are apparent in Figs. 3 and 5. The CTAB–NaSal solution strain hardens more quickly than the CPyCl–NaSal at any measured strain rate, but ruptures at a considerably lower elastic tensile stress. It is this behavior that provides the clearest insight into the fluctuating pressure drop, the time sensitive PIV and complex FIB results.

At low Deborah numbers, both fluids exhibit similar responses: symmetric streamlines, and a linear increase in pressure drop with increasing Deborah number. The FIB measurements likewise show similarity, as seen in Figs. 12 and 14. At moderate Deborah numbers, where the response is dominated by shear thinning, the steady shear rheology of the two fluids seen in Fig. 4 explains the proximity of their normalized pressure drop response, seen in Fig. 8, as the extent of the change in viscosity over two decades in shear rate is quite similar. The streaklines and PIV results of the two fluids in this regime are very similar, and the FIB patterns reveal that at comparable Deborah numbers, the two fluids show similar levels of micelle configurational changes. However, at higher Deborah numbers the extensional rheology begins to become increasingly important to the fluid dynamic response of the fluids. The time transient pressure drop of the CPyCl–NaSal shows no temporal instability, and the PIV and FIB reinforce this; even over a large time period of correlation the PIV results remain constant. The FIB indicates a growth of a strong extensional wake behind the cylinders as the fluid progresses downstream, indicating that the effects of strain hardening should impact the flow as the Deborah number is increased. This rheological prediction is born out in the normalized pressure drop data, where after a Deborah number of $De = 6$, there is an inflection point and the normalized pressure drop begins to increase sharply for increasing Deborah number. This is strong evidence that the influence of strain hardening is outpacing the shear thinning of the fluid. In the case of the CTAB–NaSal solution, the time transient pressure drop measurements begin to fluctuate with large excursions from an average value which increases with Deborah number. By examining the FIB, it is clear that under such flow conditions, the fluid does indeed experience large deformation. So much, in fact, that it becomes impossible to calculate a quantitative value of micellar deformation because the birefringence goes through so many orders. However, the birefringence does show that the patterns are no longer similar between the two fluids with increasing Deborah number, but instead the CTAB–NaSal solution exhibits spatio-temporal dependence. Examining the extensional rheology, a dramatic rupture event is observed following significant strain hardening of that filament. However at the extension rates and strains accumulated by the micelle solutions in the wake of the cylinder only the CTAB–NaSal solution was observed to rupture. The CPyCl–NaSal solution continues to strain harden for extension rates and strains well beyond the flow conditions tested in these experiments. If this were a purely elastic flow instability as has been observed for polymer solutions flowing past a single cylinder one would expect both fluids to become unstable at roughly the same Deborah number [16,20,21,23,25,29,34]. Our test solutions do not go unstable at a similar Deborah number, indicating that the instability observed is not purely elastic in nature, and is thus related to the rupture of the wormlike micelles in the wake of the circular cylinders. In a confined flow such as this, these discrete rupture events would lead to fluctuations of the pressure drop. Similar instabilities were observed during the sedimentation of spheres in wormlike micelle solutions [15,16]. Further evidence for this comes from the PIV results obtained, where it can be seen that the bulk flow direction changes over a period of time on the order of the dominant frequency of oscillation seen in the pressure drop data. In conclusion, our complete characterization of the two fluids has allowed for the observation of the interplay of fluid properties and kinematics generated by the flow of micellar solutions through a periodic array of cylinders.

References

[1] V.J. Anderson, J.R.A. Pearson, E.S. Boek, The rheology of worm-like micellar fluids, in: D.M. Binding, K. Walters (Eds.), Rheology Reviews, The British Society of Rheology, 2006.
[2] S. Kefi, J. Lee, T. Pope, P. Sullivan, E. Nelson, A. Hernandez, T. Olsen, M. Parlar, B. Powers, A. Roy, A. Wilson, A. Twynam, Expanding applications for viscoelastic surfactants, Oilfield Review (2004) 10–16.
[3] J.L. Zakin, N.W. Bewerdorff, Surfactant drag reduction, Reviews in Chemical Engineering 14 (1998) 253–320.
[4] J.N. Israelachvili, Intermolecular and Surface Forces: With Applications to Colloidal and Biological Systems, Academic Press, London, 1985.
[5] R.G. Larson, The Structure and Rheology of Complex Fluids, Oxford University Press, New York, 1999.

[6] H. Rehage, H. Hoffmann, Viscoelastic surfactant solutions: model systems for rheological research, Molecular Physics 74 (1991) 933–973.
[7] P. Schurtenberger, R. Scartazzini, L.J. Magid, M.E. Leser, P.I. Luisi, Structural and dynamic properties of polymer-like reverse micelles, Journal of Physical Chemistry 94 (1990) 3695–3701.
[8] S.-H. Tung, Y.-E. Huang, S.R. Raghavan, A new reverse wormlike micellar system: mixtures of bile salt and lecithin in organic liquids, Journal of American Chemical Society 128 (2006) 5751–5756.
[9] R.G. Laughlin, The Aqueous Phase Behavior of Surfactants, Academic Press, New York, 1994.
[10] J. Appell, G. Porte, A. Khatory, F. Kern, S.J. Candau, Static and dynamic properties of a network of wormlike surfactant micelles (etylpyridinium chlorate in sodium chlorate brine), Journal of Physics II 2 (1992) 1045–1052.
[11] S. Lerouge, J.P. Decruppe, Correlations between rheological and optical properties of a micellar solution under shear banding flow, Langmuir 16 (2000) 6464–6474.
[12] E. Miller, J.P. Rothstein, Transient evolution of shear banding in wormlike micelle solutions, Journal of Non-Newtonian Fluid Mechanics 143 (2007) 22–37.
[13] J.P. Rothstein, Transient extensional rheology of wormlike micelle solutions, Journal of Rheology 47 (2003) 1227–1247.
[14] A. Bhardwaj, E. Miller, J.P. Rothstein, Filament stretching and capillary breakup extensional rheometry measurements of viscoelastic wormlike micelle solutions, Journal of Rheology 51 (2007) 693–719.
[15] S. Chen, J.P. Rothstein, Flow of a wormlike micelle solution past a falling sphere, Journal of Non-Newtonian Fluid Mechanics 116 (2004) 205–234.
[16] J.R. Gladden, A. Belmonte, Motion of a viscoelastic micellar fluid around a cylinder: flow and fracture, Physics Review Letters 98 (2007).
[17] G.H. Mckinley, R.C. Armstrong, R.A. Brown, The wake instability in viscoelastic flow past confined circular-cylinders, Philosophical Transactions of the Royal Society of London Series a Mathematical Physical and Engineering Sciences 344 (1993) 265–304.
[18] C. Chmielewski, K. Jayaraman, Elastic instability in cross-flow of polymer-solutions through periodic arrays of cylinders, Journal of Non-Newtonian Fluid Mechanics 48 (1993) 285–301.
[19] K.K. Talwar, B. Khomami, Flow of viscoelastic fluids past periodic square arrays of cylinders—inertial and shear thinning viscosity and elasticity effects, Journal of Non-Newtonian Fluid Mechanics 57 (1995) 177–202.
[20] F.P.T. Baaijens, S.H.A. Selen, H.P.W. Baaijens, G.W.M. Peters, H.E.H. Meijer, Viscoelastic flow past a confined cylinder of a low density polyethylene melt, Journal of Non-Newtonian Fluid Mechanics 68 (1997) 173–203.
[21] H.P.W. Baaijens, G.W.M. Peters, F.P.T. Baaijens, H.E.H. Meijer, Viscoelastic flow past a confined cylinder of a polyisobutylene solution, Journal of Rheology 39 (1995) 1243–1277.
[22] H. Usui, T. Shibata, Y. Sano, Karman vortex behind a circular-cylinder in dilute polymer-solutions, Journal of Chemical Engineering of Japan 13 (1980) 77–79.
[23] S.A. Dhahir, K. Walters, On non-Newtonian flow past a cylinder in a confined flow, Journal of Rheology 33 (1989) 781–804.
[24] J.M. Verhelst, E.M. Nieuwstadt, Visco-elastic flow past circular cylinders mounted in a channel: experimental measurements of velocity and drag, Journal of Non-Newtonian Fluid Mechanics 116 (2004) 301–328.
[25] S. Ogata, Y. Osano, K. Watanabe, Effect of surfactant solutions on the drag and the flow pattern of a circular cylinder, AIChE Journal 52 (2006) 49–57.
[26] A. Liu, Viscoelastic flow of polymer solutions around arrays of cylinders: comparison of experiment and theory, Ph.D. Thesis, MIT Dept. Chemical Engineering, 1997.
[27] A.W. Liu, D.E. Bornside, R.C. Armstrong, R.A. Brown, Viscoelastic flow of polymer solutions around a periodic, linear array of cylinders: comparisons of predictions for microstructure and flow fields, Journal of Non-Newtonian Fluid Mechanics 77 (1998) 153–190.
[28] R.J. Marshall, A.B. Metzner, Flow of viscoelastic fluids through porous media, Industrial & Engineering Chemistry Fundamentals 6 (1967) 393–400.
[29] M.A. Hulsen, R. Fattal, R. Kupferman, Flow of viscoelastic fluids past a cylinder at high Weissenberg number: stabilized simulations using matrix logarithms, Journal of Non-Newtonian Fluid Mechanics 127 (2005) 27–39.
[30] M.D. Smith, Y.L. Joo, R.C. Armstrong, R.A. Brown, Linear stability analysis of flow of an Oldroyd-B fluid through a linear array of cylinders, Journal of Non-Newtonian Fluid Mechanics 109 (2003) 13–50.
[31] P.J. Oliveira, A.I.P. Miranda, A numerical study of steady and unsteady viscoelastic flow past bounded cylinders, Journal of Non-Newtonian Fluid Mechanics 127 (2005) 51–66.
[32] K. Arora, R. Sureshkumar, B. Khomami, Experimental investigation of purely elastic instabilities in periodic flows, Journal of Non-Newtonian Fluid Mechanics 108 (2002) 209–226.
[33] E.H. Wissler, Viscoelastic effects in flow of non-newtonian fluids through a porous medium, Industrial & Engineering Chemistry Fundamentals 10 (1971) 411–417.
[34] O. Manero, B. Mena, On the slow flow of viscoelastic liquids past a circular-cylinder, Journal of Non-Newtonian Fluid Mechanics 9 (1981) 379–387.
[35] G.G. Maitland, Oil and gas production, Current Opinion in Colloid and Interface Science 5 (2000) 301–311.
[36] B. Chase, W. Chmilowski, Y. Dang, Clear fracturing fluids for increase well productivity, Oilfield Review (1997) 20–33.
[37] C.L. Perrin, P.M.J. Tardy, K.S. Sorbie, J.C. Crawshaw, Experimental and modeling study of Newtonian and non-Newtonian fluid flow in pore network micromodels, Journal of Colloids and Interface Science 295 (2006) 542–550.
[38] A.J. Muller, M.F. Torres, A.E. Saez, Effect of the flow field on the rheological behavior of aqueous cetyltrimethylammonium *p*-toluenesulfonate solutions, Langmuir 20 (2004) 3838–3841.
[39] R.P. Chhabra, Bubbles, Drops and Particles in Non-Newtonian Fluids, CRC Press, Boca Raton, 2007.
[40] C.M. DaRocha, L.G. Patruyo, N.E. Ramĭrez, A.J. Muller, A.E. Saez, Polymer Bulletin 42 (1999) 109–116.
[41] T. Koshiba, T. Hashimoto, N. Mori, T. Yamamoto, Pressure loss of viscoelastic surfactant solutions under the flow in a packed bed of particles, Nihon Reoroji Gakkaishi 35 (2007) 21–26.
[42] M.R. Rojas, A.J. Muller, A.E. Saez, Shear rheology and porous media flow of wormlike micelle solutions formed by mixtures of surfactants of opposite charge, Journal of Colloid and Interface Science 326 (2008) 221–226.
[43] E.S. Boek, J.T. Padding, V.J. Anderson, W.J. Briels, J.P. Crawshaw, Flow of entangled wormlike micellar fluids: Mesoscopic simulations,rheology and μ-PIV experiments, Journal of Non-Newtonian Fluid Mechanics 146 (2007) 11–21.
[44] J.P. Rothstein, G.H. McKinley, The axisymmetric contraction-expansion: the role of extensional rheology on vortex growth dynamics and the enhanced pressure drop, Journal of Non-Newtonian Fluid Mechanics 98 (2001) 33–63.
[45] L.E. Rodd, T.P. Scott, D.V. Boger, J.J. Cooper-White, G.H. McKinley, The inertio-elastic planar entry flow of low-viscosity elastic fluids in micro-fabricated geometries, Journal of Non-Newtonian Fluid Mechanics 129 (2005) 1–22.
[46] T. Koshiba, N. Mori, K. Nakamura, S. Sugiyama, Measurement of pressure loss and observation of the flow field in viscoeastic flow through undulating channels, Journal of Rheology 44 (2000) 65–78.
[47] G.G. Fuller, Optical Rheometry of Complex Fluids, Oxford University Press, New York, 1995.
[48] E.K. Wheeler, P. Fischer, G.G. Fuller, Time-periodic flow induced structures and instabilities in a viscoelastic surfactant solution, Journal of Non-Newtonian Fluid Mechanics 75 (1998) 193–208.
[49] T. Shikata, S.J. Dahman, D.S. Pearson, Rheo-optic behavior of wormlike micelles, Langmuir 10 (1994) 3470–3476.
[50] F. Kern, F. Lequeux, R. Zana, S.J. Candau, Dynamics properties of salt-free viscoelastic micellar solutions, Langmuir 10 (1994) 1714–1723.
[51] J.Y. Lee, G.G. Fuller, N.E. Hudson, X.-F. Yuan, Investigation of shear-banding structure in wormlike micellar solution by point-wise flow-induced birefringence measurements, Journal of Rheology 49 (2005) 537–550.
[52] R.B. Bird, R.C. Armstrong, O. Hassager, Dynamics of Polymeric Liquids: Volume 1. Fluid Mechanics, John Wiley & Sons, New York, 1987.
[53] P. Fischer, H. Rehage, Rheological master curves of viscoelastic surfactant solutions by varying the solvent viscosity and temperature, Langmuir 13 (1997) 7012–7020.
[54] M.E. Cates, Reptation of living polymers: dynamics of entangled polymers in the presence of reversible chain-scission reactions, Macromolecules 20 (1987) 2289–2296.
[55] M. Doi, S.F. Edwards, The Theory of Polymer Dynamics, Oxford University Press, Oxford, 1986.
[56] R. Granek, M.E. Cates, Stress relaxation in living polymers: results from a Poisson renewal model, J. Chem. Phys. 96 (1992) 4758–4767.
[57] E. Fischer, P.T. Callaghan, Shear banding and the isotropic-to-nematic transition in wormlike micelles, Phys. Rev. E 64 (2001) 011501.
[58] E. Cappelaere, J.-F. Berret, J.P. Decruppe, R. Cressely, P. Lindner, Rheology, birefringence, and small angle neutron scattering in a charged micellar system: evidence of shear-induced phase transition, Phys. Rev. E 56 (1997) 1869–1878.
[59] J. Drappier, D. Bonn, J. Meunier, S. Lerouge, J.P. Decruppe, F. Bertrand, Correlation between birefringent bands and shear bands in surfactant solutions, Journal of Statistical Mechanics: Theory and Experiments (2006) P04003.
[60] A. Bhardwaj, D. Richter, M. Chellamuthu, J.P. Rothstein, The effect of pre-shear on the extensional rheology of wormlike micelle solutions, Rheologica Acta 46 (2007) 861–875.
[61] F.J. Alcocer, V. Kumar, P. Singh, Permeability of periodic porous media, Physical Review E 59 (1999) 711–714.
[62] F.J. Alcocer, P. Singh, Permeability of periodic arrays of cylinders for viscoelastic flows, Physics of Fluids 14 (2002) 2578–2581.
[63] C. Chmielewski, C.A. Petty, K. Jayaraman, Cross-flow of elastic liquids through arrays of cylinders, Journal of Non-Newtonian Fluid Mechanics 35 (1990) 309–325.
[64] C. Chmielewski, K. Jayaraman, The effect of polymer extensibility on cross-flow of polymer-solutions through cylinder arrays, Journal of Rheology 36 (1992) 1105–1126.
[65] J.M. Kim, C. Kim, C. Chung, K.H. Ahn, S.J. Lee, Negative wake generation of FENE-CR fluids in uniform and Poiseuille flows past a cylinder, Rheologica Acta 44 (2005) 600–613.
[66] A. Afonso, M.A. Alves, F.T. Pinho, P.J. Oliveira, Uniform flow of viscoelastic fluids past a confined falling cylinder, Rheologica Acta 47 (2008) 325–348.